Asynchronous Invariant Digital Image Watermarking in Radon Field for Resistant Encrypted Watermark

Dhekra Essaidani, Hassene Seddik, and Ezzedine Ben Braiek
(Corresponding author: Dhekra Essaidani)
Product Research Center, CEREP Research Laboratory, ESSTT
5 Av. Taha Hussein, 1008, Tunis
(Email: dhekraessaidani89@gmail.com)
(Received Aug. 19, 2013; revised and accepted Jan 10 & Mar. 15, 2014)

Abstract

With the rapid evolution of processing multimedia technologies (text, audio, image and video) and its internet application (wide and easy transmission of digital multimedia contents), the copyright protection has been receiving an increasing attention. Among the existing strategies to protect multimedia online, digital watermarking provides a promising way of protecting data online from illegal manipulation and duplication. In this paper, a new image of watermarking scheme is presented. It performs imperceptible watermarking of color image in the radon domain. The proposed algorithm can resist to geometrical attacks. Experimental results show that the proposed watermarking approach not only can meet the demand on invisibility and robustness of the watermark, but also presents a good performance compared to other proposed methods considered in the comparative study. A mathematical study is developed to demonstrate how and why this approach is robust against geometric transforms.

Keywords: Asynchronous attacks, circular integration transform (CIT), color image watermarking, discrete radon transform, radial integration transform (RIT), robustness

1 Introduction

The rapid development of processing data technologies and internet applications has improved the ease of access to information online. It also increases the problem of illegal copying and redistribution of digital media. Encryption and Stenography are the two techniques introduced to solve data on line. In 1992, the research suggested to use the watermarking technique in data protection.

Nowadays, image watermarking is a protection technology that has attracted a lot of attention. The basic idea of watermarking involves integrating a message into a digital content. This last covers the information to be transmitted in a holder in a way to be invisible and correctly reversible (an algorithm allows the exact extraction of the embedded watermark). Its algorithm requires equilibrium between three constraints: imperceptibility, robustness and embedding capacity [2].

Image watermarking schemes have to keep the image quality and to be robust against general image processing and geometric transformation (scaling, rotation and translation) [15]. There are many watermarking algorithms which have been presented in recent literature to protect data against geometric attacks. They can be divided in three main categories. The first one includes watermarking approach which is a watermark detection performing in an invariant domain to geometric attacks. The second category includes methods that detect and correct the geometric attack of the watermarked image in order to perform the detection process. However, another approach for resisting geometric attacks is based on synchronizing, in terms of position, orientation and scaling, use image features to embed and extract the correlating watermark [13].

Various watermarking schemes are proposed for the digital multimedia protection. Most of the schemes perform on the spatial domain where the watermarking techniques directly modify the intensities of selected pixels [4, 5, 6, 8, 9]. Also, several schemes perform on the transformation domain (Fourier-Mellin Transform, Discrete Cosine Transform (DCT), Discrete Fourier Transform (DFT), Discrete Wavelet Transform and the Complex Wavelet Transform (CWT)) where the watermarking algorithm modifies the selected transformed coefficients [10, 16, 18]. In [18], authors used the properties of Fourier transform to develop a watermarking scheme resisting the unavoidable noise and cropping. This algorithm presents a robust watermark strategy for quantum images. The watermark is embedded into the Fourier coefficients of the quantum carrier image. Authors in [15]

proposed a state-coding based on blind watermarking algorithm to embed color image watermark to color host image. This approach used the Integer Wavelet Transform (IWT) and the rules of state coding of the components, R, G and B, of color image watermark and the components, Y, Cr and Cb, of color host image. In the extraction process, authors used also the rules of state coding to recover the original watermark or original host image. In [11], authors proposed an invariant image watermarking scheme by introducing the Polar Harmonic Transform (PHT). This algorithm proposed to resist geometric transformation. Furthermore, Xiao, Ma and Cui have been used for invariance watermarking scheme against global geometric that transforms the Radon field and pseudo-Fourier-Mellin transforms. This combination is named Radon and pseudo-Fourier-Mellin invariants (RPFMI) [17].

In order to resist geometric attacks, we propose a new watermarking algorithm for RGB color image. The proposed approach belongs to the second of the categories that were described above. Imperceptible watermark embedding and detection are performed in the non-conventional radon domain. Our approach selects specific coefficients based on their energy in Radon field to embed watermark. The simulation results proved by mathematical study proved the high efficiency and robustness of the proposed approach. This paper is organized as follows: Section 2 presents an overview of Radon Transformation (RT). Section 3 details our watermarking method. In Section 4, we study the robustness of this technique against different STIRMARK attacks, and we test the ability to detect the embedded watermark in the host image. A study of the watermarked image distortions before and after different attacks is also presented. In Section 5, a mathematical study is developed to explain the resistance of the proposed method and prove the results found. A comparative study with recent published techniques is also presented.

2 Mathematical Recall of Radon Transform

2.1 Generalized Radon Transform

In 1917, Radon, Austrian mathematician, defined the theory of Radon Transform. He proved the possibility to reconstruct a function of a space from knowledge of its integration along the hyper-plans in the same space. This theory establishes the reversibility of the Radon transform and the transition between the native function space and the Radon space, or the space of projections [3]. In image processing, the Radon Transform represents a collection of projections along various directions [14]. The generalized Radon transformation of a 2D continuous function is defined in [1] by the following equation:

$$R(\rho,\theta)=\int_{-\infty}^{+\infty}\int_{-\infty}^{+\infty} f(x,y)\delta(x\cos\theta+y\sin\theta-\rho)dxdy,$$

where ρ represents the perpendicular distance of a straight line from the origin, and represents the angle between the distance vector and the x-axis.

The literature proposed two categories of one-dimensional Radon transformation; the first is based on Radial Integration Transform (RIT) and the second is based on the Circular Integration Transform (CIT).

2.1.1 One-Dimensional Radial Integration Transform

The RIT of a function $f(x,y)$ is defined as the integral of $f(x,y)$ along a straight line that begins from the origin $(x_0,y_0)$and has angle θ with respect to the horizontal axis (see Figure 1). It is given by the following equation [13]:

$$R_f(\theta)=\int_0^{+\infty} f(x_0+u\cos\theta, y_0+u\sin\theta)du,$$

where u is the distance from the origin $(x_0,y_0)$and $f(x,y)$ is presented by the integral along a straight line that begins from the origin (x_0,y_0) and has an angle with respect to the horizontal axis.

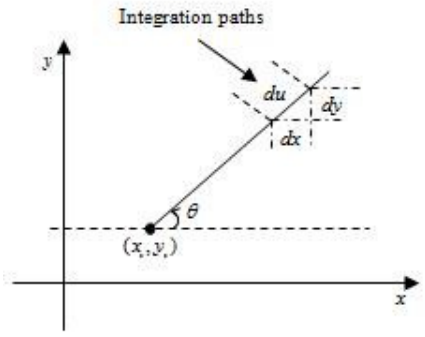

Figure 1: Representation of the radial integration transform

2.1.2 One-Dimensional Circular Integration Transform

The CIT of a function $f(x,y)$ is defined as the integral of $f(x,y)$ along a circle curve with center x_0,y_0 and radius ρ(see Figure 2). It is given at [13] by the following equation:

$$C_f(\rho)=\int_0^{2\pi} f(x_0+\rho\cos\theta, y_0+\rho\sin\theta)\rho d\theta,$$

where $d\theta$ is the corresponding elementary angle and $f(x,y)$ represents the circle integrated function around the center $(x_0,y_0)$and by the radius ρ.

2.2 Discrete Radon Transform (DRT)

The discreet Radon transformation 'DRT' of an image $I(x,y)$ can be defined by the following equations [13]:

$$R(t\Delta\theta)=\tfrac{1}{J}\sum_{j=1}^{J} I(x_0+j\Delta s\cos(t\Delta\theta), y_0+j\Delta s\sin(t\Delta\theta)).$$

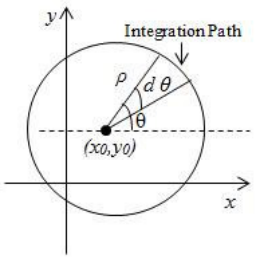

Figure 2: Representation of the circular integration transform

$$C(k\Delta\rho) = \frac{1}{T}\sum_{t=1}^{T} I(x_0 + k\Delta\rho\cos(t\Delta\theta), \\ y_0 + k\Delta\rho\sin(t\Delta\theta)),$$

where $d\theta$ represents the angular variation step, Δs is the scaling step, $k\Delta p$ represents the radius of the smallest circle that encircles the image, J represents the number of samples on the radius with orientation θ, $t = 1, ..., \frac{360}{\Delta\theta}$ and $k = 1, ..., \frac{360}{\Delta\theta}$.

The Radon transformation of the image $I(x, y)$ of size $[MN]$ generate a matrix $R(\rho, \theta)$ of a size equal to N_ρ, N_e with real coefficient representing the radon filed with:

$$\begin{cases} N_\rho &= \sqrt{N^2 + M^2} + 1 \\ M_\rho &= \frac{\theta_{\max}}{\Delta\theta}. \end{cases} \quad (1)$$

3 The Proposed Watermarking Approach

The literature suggested that the Radon Transform properties are much recommended in watermarking applications in which resistance to geometric attacks. A watermark embedding and detection scheme using these properties are described in the proposed watermarking approach. Also, due to the expansion of the projected image matrix from its size $[M, N]$ to $[M_\rho, N_e]$ this filed allows a higher amount of embedded data. In fact the DRT increases the size of the transformed image (see Equation (1)). The proposed method consists in embedding the watermark in selected coefficients in the radon field. These coefficients are chosen from the area of maximal energy. They represent maxims in the Radon coefficients and must respect the following three essential characteristics:

- These coefficients are set on the integral line of projection, so they will be well recovered from the inverse radon transform.
- Secondly, they contain the most important details of the original images. Consequently, they are the most adapted to a code in a watermark with better imperceptibility.
- Their high values enable us to hide the binary coefficients of the watermark without any perceptual degradation.

3.1 Details of the Proposed Algorithm

In the following Sections, we will note the original watermark as W_o, the encrypted embedded watermark as W, the recovered encrypted watermark as $W^{'}$,the recovered decrypted watermark as $W_o^{'}$, the Original RGB color image (support or host image) as I, the original blue matrix of the host image as I_b,the transformed channel blue (matrix blue) of the host image in Radon field as R_b, the watermarked channel blue (matrix blue) of the host image in Radon field as R_{bw}, the watermarked blue matrix in spatial field as I_{bw}, I_w represents the watermarked spatial image and the transformed channel blue (matrix blue) of the watermarked host image in Radon field as $R_{bw}^{'}$. Likewise, (x, y) represents the spatial coordinates of the original image, (ρ, θ) represents the coordinates of the color image in the radon field and k and l are the coded bits representing the watermark, $[M_w\, N_w]$ represents the size of the original image, $[M\, N]$represents the size of original watermark, $[N_\rho\, N_\theta]$ represents the size of the image in radon domain and G is the embedding strength.

3.1.1 Watermark Embedding Process

The main concept of the watermark embedding process is shown in Figure 3.

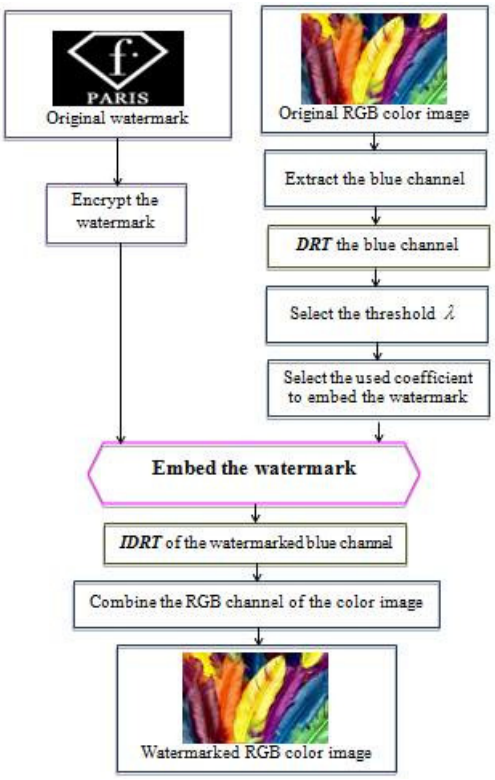

Figure 3: Watermarking algorithm

For the RGB color image, the red, green and blue channels are candidates for watermark embedding as human eyes are not sensitive on the modification of blue channel than the green and red channels. Besides, Watermarking in the blue channel allows good invisibility and higher

embedding capacity. Therefore, we propose to embed the watermark in the blue channel of the selected color image [7]. The proposed algorithm is described in the following steps:

Step 1: Encrypt the watermark.

In order to encrypt the watermark, we use the following steps:

1) Transform the original watermark W_o into a one dimensional vector V_{water} by the following equation:

$$W_o(x,y) \rightarrow V_{water}(l).$$

2) Decompose the watermark in N equal blocks B_i, where

$$V_{water}(N) = \{B_1, B_2, ..., B_N.$$

3) Generate a key $key0$ witch its length is equal to the length of the block B_i.

4) Encrypt the first block B_1 by using the following equation:

$$Bc_1 = B_1 \oplus key0.$$

5) Encrypt the second block B_2 by using the following equation:

$$Bc_2 = B_2 \oplus Bc_1.$$

6) Generally, after each encrypting iterates of each block B_i , the resulting encrypted blocks Bc_i is used to encrypt the next block Bc_{i+1}, where $i = 3, 4, 5, ..., N$.

$$Bc_i = B_i \oplus Bc_{i-1}.$$

7) After encrypting the watermark by using the function "XOR", we applied S_{max} iteratively permutations on the encrypted watermark vector in order to improve the encryption system. The first permutated iteration is defined by the following equation:

$$P_{s=1}(B_1, ..., B_N) = W_o : B_{N/2}, ..., B_1, B_N, ..., B_{((N/2)+1)}.$$

We continue the permutation process by applying the defined function as follows:

$$P_{s=\alpha}(Bc_1, ..., Bc_N) = P_{s=\alpha-1}Bc_N, ..., Bc_{(N/2)}, Bc_1, ..., Bc_{((N/2)+1)},$$

where $\alpha = 2 \rightarrow S_{max}$ and S_{max} represents the number of the permutation iteration. The encrypted watermark vector V_c is obtained after S_{max} permutations and it is defined as follows:

$$V_c(l) = P_{s=20}(l).$$

To obtain the encrypted watermark, we transformed the vector V_c to matrix with size equal to $[M_w\ N_w]$ defined as follows:

$$V_c(l) \rightarrow W(x,y).$$

Step 2: Select the radon coefficients to embed the watermark.

In this step, a discrete radon transform is applied only on the blue channel I_b of the color image I. A selection of a set of coefficients having the higher energy from this transformed matrix called R_b is done. The number of the selected coefficient is equal to $M_w \times N_w$ which represents the length of the encrypted watermark. For this reason, we transform the image matrix into a vector V by using the following equation:

$$Rb(\rho, \theta) \rightarrow V(k).$$

Then, the vector V is organized in downward order. It is defined as fellows:

$$V(1) > V(2) > V(3) > ... > V(k-1) > V(k),$$

where $K = M_\theta * N_\theta$ Next, we select the used coefficients to embed the watermark. They represent the $M_w \times N_w$ first highest coefficients in the matrix R_b. For this process, we use the following steps:

1) Define the threshold λ_{opt} : It represents the coefficient number $M_w \times N_w$ in the vector V:

$$\lambda_{opt} = V(M_w * N_w).$$

2) Select the coefficients to be used for watermark coding:

$$R_E(\rho, \theta) = R_b(\rho, \theta) \qquad where R_b(\rho, \theta) \geq \lambda_{opt}.$$

So, the selected coefficient to encode the watermark represent the $M_w \times N_w$ first coefficients in the vector V:

$$R_E(\rho, \theta) = V(l).$$

Step 3: Embedding process.

The embedding process is described in Figure 4.

Each selected coefficient coded one bits of the encrypted watermark vector V_w. To embed watermark in the selected coefficient of the matrix R_b, we used the following equation:

$$\begin{cases} R_{bw}(\rho, \theta) = R_b(\rho, \theta) + G & if \ \ V_c(l) = 1 \\ R_{bw}(\rho, \theta) = R_b(\rho, \theta) - G & if \ \ V_c(l) = 0. \end{cases}$$

Also, we use the vectors Er, E_ρ and E_θ to save the amplitude, the position ρ and the position θ of each selected coefficient $R_b(\rho, \theta)$. These vectors have the length $M_w \times N_w$. They are used later to recover the embedding watermark. These vectors are filled by using the following equations:

$$Er(c) = R_b(\rho, \theta).$$

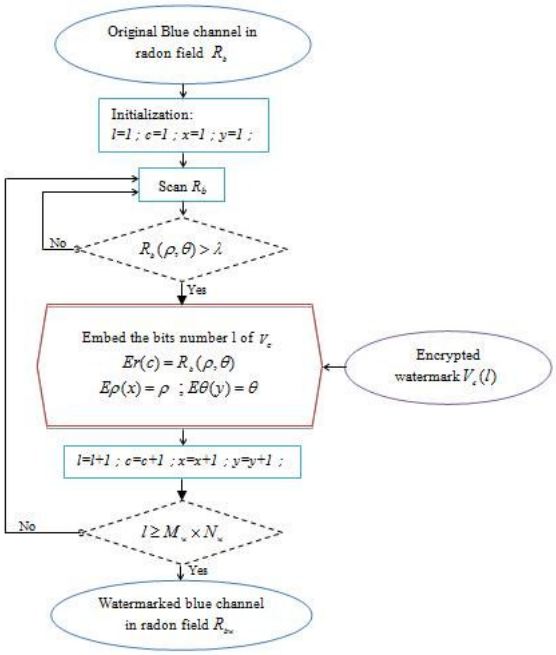

Figure 4: Embedding process

$$\begin{cases} E_\theta(y) = \theta \\ E_\rho(x) = \rho. \end{cases}$$

Step 4: Watermarking image in spatial field.

We transform the watermarking blue matrix R_{bw} by the inverse DRT (IDRT) and we combine the RGB channels of the image to create the watermarked color image in spatial domain I_w.

3.1.2 Watermark Recovering Process

This algorithm represents the second principal algorithm in every watermarking approach. It serves to recover the embedded information with minimal loss. For this reason, it is necessary to respect the used parameter of the processing field and to use the details of the embedding program in this approach. This process is detailed by the illustrated in Figure 5.

In this algorithm, we extract the blue channel I_{bw}.Then, we apply a radon transform with the same parameter used in the embedding process (step2 and step 3 in paragraph 3.1.1) for the extracted channel. This transformation gives the watermarked blue channel in radon field R'_{bw}. Next, we use the two saved vectors E_ρ and E_θ detect the position of the used coefficient to embed the encrypted watermark. The amplitudes of the detecting coefficients are saved in the vector E'_r by using the following equation:

$$Er'(cl) = R'_{bw}(E_\rho(cl), E_\theta(cl)),$$

where $cl = 1, 2, 3, ..., M_w \times N_w$ This vector contains the used coefficients in embedding the watermark. In order to decide if the embedding bits is equal to 1 or 0. We

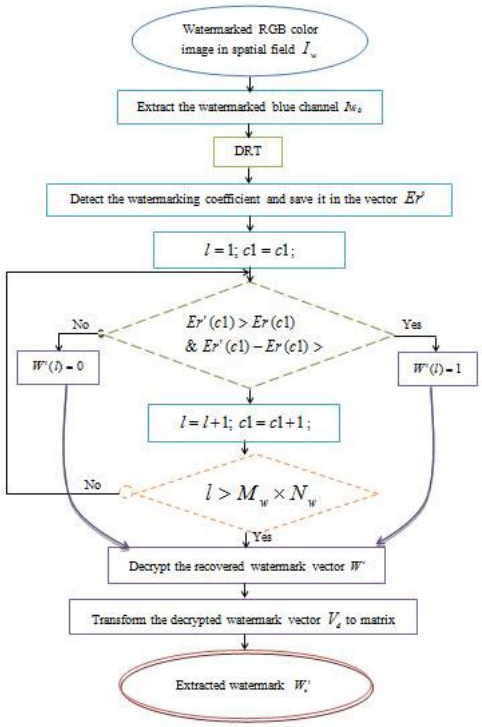

Figure 5: Watermark extraction process

compare the two saved vectors E'_r and E_r bit by bits and its difference with the selected threshold T. In this step, we use the comparison test defined as follows:

$$\begin{cases} W'(l) = 1 \; if Er(l) \geq Er'(l) \, and \; Er'(l) - Er(l) > T \\ W'(l) = 0 \; else. \end{cases}$$

The recovered watermark W' is a one-dimensional vector which represents the encrypted watermark. To decrypt it, we use the same algorithm used to encrypt the original watermark with the same parameters and steps. It is defined as follows:

1) Decompose the recovered encrypted watermark vector in N equal blocks B'_i with length equal to the length of the blocks B_i where $i = 1, 2, ..., N$:

$$V'_{water}(N) = B'_1, B'_2, ..., B'_N.$$

2) In order to recover the original watermark, we apply S_{max} iteratively inverses permutations to the recover encrypted watermark vector.The first inverse permutation is defined as follows:

$$P^{-1}_{S'=1}(B'_1, B'_2, ..., B'_N) = V'_{water}(B'_{((N/2)+1}, ..., B'_N, B'_{(N/2)}, ..., B'_1).$$

The next of the inverse permutation process defined by the following equation:

$$P^{-1}_{S'=\alpha}(B'_1, B'_2, ..., B'_N) = P^{-1}_{S'=\alpha-1}(B'_{((N/2)+1}, ..., B'_N, B'_{(N/2)}, ..., B'_1),$$

where $\alpha = 2 \rightarrow S_{max}$ and S_{max} represents the number of the permutation iteration used in the embedding watermark process. The decrypted watermark vector after S_{max} inverse permutation V_d it is defined as follows:

$$V_d(l) = P^{-1}_{S=S_{max}}(l).$$

3) Devise V_d into blocks $B_i^{'}$ with equal length equal to the length of the blocks B_i where $i = 1, 2, ..., N$. Use the same key sing in the embedding process $key0$ to decrypt the first block Br_1 by using the following equation:

$$Br_1 = B_1^{'} \oplus key0.$$

4) Decrypt the second block $B_2^{'}$ by using the following equation:

$$Br_2 = B_2^{'} \oplus B_1^{'}.$$

5) Generally, after each decrypting iterates of each block Br_i, the resulting decrypted blocks is used to decrypt the next block Br_{i+1} where $i = 3, 4, ..., N-1, N$.

$$Br_i = B_i^{'} \oplus B_{i-1}^{'}.$$

6) The decrypted watermark after application of XOR function is defined as follows:

$$V_d^{'}(N) = Br_1, Br_2, ..., Br_N.$$

Finally, to obtain the decrypted watermark, we transformed the vector V_d to matrix with size equal to $[M_w N_w]$ defined as follows:

$$V_d^{'}(N) \rightarrow W_O^{'}(x, y).$$

$W_o^{'}$ is the recover watermark.

3.2 Experimental Results

To evaluate the performance of the proposed watermarking scheme, we use a data base composed with 100 logical watermarks coded on 0 and 1 binary ($d = 2$) and 50 host cover images. Different tests give results close to the present results in this paper. In this work, we present the results of the standard Lena image RGB color (see Fig.18) with size (256×256) and a watermark with a size (80×80) (see Figure 20). We apply a discrete radon transform to the original image with an integration angle path "in degree $\Delta\theta = 1$ for $\theta \in [02\pi]$ and an integration scale path $\Delta\rho = 1 pixels$ for $\rho \in [0\sqrt{M^2 + N^2} + 1]$.

The similitude rate between the extracted watermark and the original watermark is continuously computed to test the robustness of this approach. This is done by the normalized Cross-correlation presented in the following equation:

$$NC = \frac{\sum_{i=1}^{M_q} \sum_{i=1}^{N_q} W_o W_o^{'}}{\sqrt{\sum_1^{M_q} [\sum_1^{N_q} W_o^2] \sum_1^{M_q} [\sum_1^{N_q} W_o^{'2}]}}.$$

On the other hand, the imperceptibility of the embedded watermark is a constraint that must be respected. A measure of similarity rate based on the PSNR described by the following equation is computed after each watermarking process with respect to the gain factor used. A threshold of $37\,dB$ is fixed to verify if some distortions begin to appear on the watermarked image in addition to a psycho-visual decision.

$$PSNR = 10 \log(\frac{d^2}{MSE}).$$

Where d represents the maximal image intensities ($d = 256$ for the host cover image and $d = 2$ for the used logical watermark in our case) and MSE is calculated in the following equation:

$$MSE = \frac{1}{M_w \times N_w} \sum_{i=1}^{M_w \times N_w} (W_o - W_o^{'})^2.$$

The first step of this simulation study consists to select the threshold λ uses to select the radon coefficients used to embed the watermark.

3.2.1 Selection of the Threshold λ

The threshold λ which is chosen for selecting the radon coefficients will be used to embed the watermark in order to improve the robustness of the proposed watermarking scheme against different attacks categories. For that purpose, it is provided in the following five different values of λ, (λ_0, λ_{min}, $\lambda_{means-inf}$,$\lambda_{means-max}$ and λ_{max}), used to select the encoding coefficients. A comparative study is performed to select the optimum threshold used to select the embedding coefficients.

1) Watermarking in coefficients equal to 0.
To select the encoded coefficients $R_E(\rho, \theta)$, we used a threshold $\lambda_0 = 0$. The number of the selected coefficient is equal to $M_w * N_w$ where:

$$if\ \mathrm{R}_b(\rho, \theta) = \lambda_0 \qquad then \qquad R_E(\rho, \theta) = R_b(\rho, \theta).$$

The simulations tests show that we cannot recover the embedding watermark in the coefficients equal to 0. So, the comparative parameters give the following results: $C = NaN$, $PSNR = NaN$ and $BER = 6400 bits = 100\%$.

2) Watermarking in minimal coefficients different to 0.
In this algorithm, the coefficients whose values are minimal and different from zero are selected. For this reason we used a counter "count" to compute the number of zero in the matrix $R_b(\rho, \theta)$:

$$\begin{cases} count = 0; \\ if\ \ R_b(\rho, \theta) = 0\ \ then\ \ count = count + 1; \\ end. \end{cases}$$

The threshold λ_{min} is selected as follows:

$$\lambda_{min} = V(((len - count) - (M_w \times N_w)) + 1),$$

where len is the length V of the vector representing the coefficients of the host radon image organized in downward order.
The selected coefficient to embed watermark are:

$$R_E(\rho,\theta) = R_b(\rho,\theta) \quad where\, R_b(\rho,\theta) \leq \lambda_{min} \quad and \quad R_b(\rho,\theta) \neq 0.$$

The simulations tests give a threshold $\lambda_{min} = 5073$ and they show that we can recover the embedding watermark by the following parameter quality results: $C = 0.3023$, $PSNR = 52.3670dB$, $BER = 2413bits = 37.70$ %. The visual results given in Figures 6 and 7.

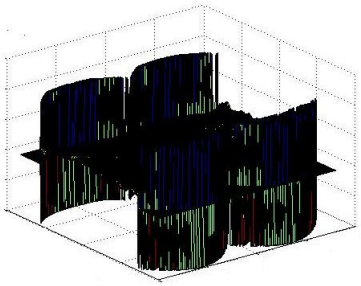

Figure 6: Watermarking image in radon field

Figure 7: Recovered watermark

3) Watermarking in maximal coefficients.
The used process to define λ_{max} is same of the defined process in step 2 of the paragraph 3.1.1 (watermark embedding process) where $\lambda_{max} = \lambda_{opt}$.

The simulations tests give a threshold $\lambda_{max} = 32208$ and they show that we can recover the embedding watermark by the following parameters quality results: $C = 1$, $PSNR = Inf$ and $BER = 0bits = 0$ %. The visual results given in Figures 8 and 9.

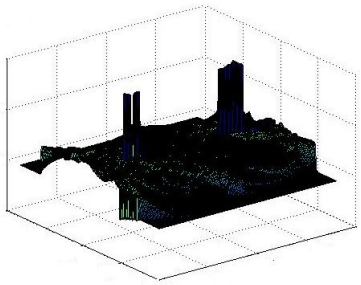

Figure 8: Watermarking image in radon field

Figure 9: Recovered watermark

4) Watermarking in the higher coefficients to λ_{means} and different to the maximal coefficients.
In this algorithm the selected coefficient to embed watermark are:

$$R_E(\rho,\theta) = R_b(\rho,\theta)$$
$$where\ R_b(\rho,\theta) > \lambda_{means}\, and\, R_b(\rho,\theta) < \lambda_{max}.$$

The used threshold in this algorithm is noted by $\lambda_{means-sup}$.The simulations results give $\lambda_{means} = \lambda_{means-sup} = 18842$ and $\lambda_{max} = 32208$. The simulation tests show that we can recover the embedding watermark by the following parameter quality results: $C = 0.9149$, $PSNR = 62.5942$ and $BER = 229bits = 3.57\%$. The visual results given in Figures 10 and 11.

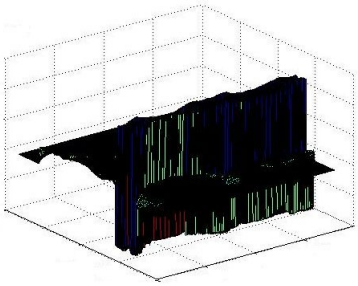

Figure 10: Watermarking image in radon field

Figure 11: Recovered watermark

5) Watermarking in the less coefficients to λ_{means} and different to the minimal coefficients.
In this algorithm the selected coefficient to embed watermark are:

$$R_E(\rho,\theta) = R_b(\rho,\theta) \quad where \quad R_b(\rho,\theta) < \lambda_{means} \quad and \quad R_b(\rho,\theta) > \lambda_{min}.$$

The used threshold in this algorithm is noted by $\lambda_{means-inf}$. The simulations results give $\lambda_{means} = \lambda_{means-inf} = 18842$ and $\lambda_{min} = 5073$. The simulation tests show that we can recover the embedding watermark by the following parameter quality results: $C = 0.7957$, $PSNR = 58.8606$ and $BER = 541bits = 8.45\%$. The visual results given Figures 12 and 13.

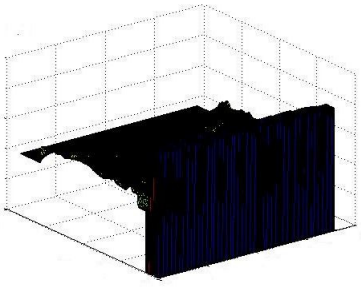

Figure 12: Watermarking image in radon field

Figure 13: Recovered watermark

6) Comparative study to select λ.

Figures 14, 15, and 16 show the variation of the correlation, PSNR and BER of the recovered watermark for different values of threshold λ.

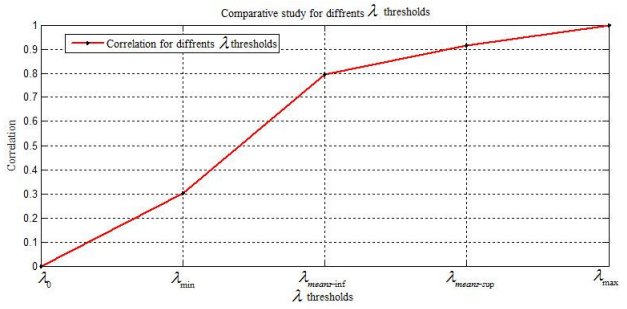

Figure 14: Correlation variation of the recovered watermark for different values of threshold λ

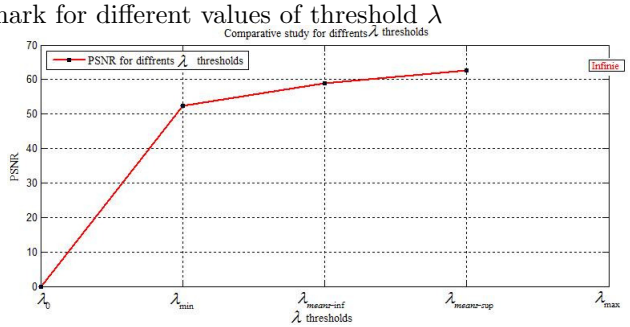

Figure 15: PSNR variation of the recovered watermark for different values of threshold λ

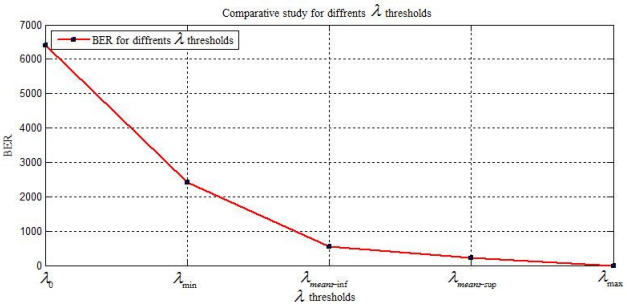

Figure 16: BER variation of the recovered watermark for different values of threshold λ

Figures 14, 15, and 16 show that the more threshold λ increases the better the correlation of the recovered watermark becomes. So, the optimum threshold λ is $\lambda_{opt} = \lambda_{max}$.Generally, the robustness of the proposed method against synchronous and asynchronous attacks for the higher coefficient depends on the highest energy of the radon region. The important peaks of radon domain are located at the points corresponding to the projection parameter. Besides, the coefficients of the radon region in which the highest energy is located and set on the line of projection contain the significant information of the original image. So, they allow a good recovery of the transformed information with inverse radon transform.

3.2.2 Robustness of the Proposed Watermarking Approach

An example of an original and a watermarked image is illustrated in Figure 17 and 18. The set of Figures 19, 20 and 21 illustrate respectively the original watermark, the encrypted one and the decrypted recovered watermark from the radon field.

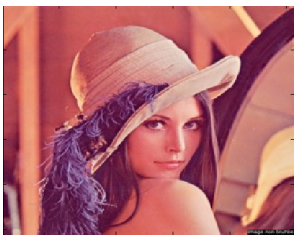

Figure 17: Original image

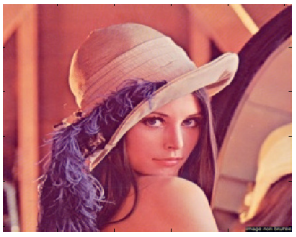

Figure 18: watermarked image

Figure 19: Original watermark

Figure 20: Encripted watermark

Figure 21: Recovered watermark

In the simulation test, we use a factor gain $G = 1000$ to embed the watermark in the selected coefficient in radon field. These coefficients are higher to $\lambda_{opt} = 32208$. This application gives a PSNR value between the original and the watermarked host image equal to $PSNR = 30.89dB$. The normalized cross-correlation between original and correlating watermark is $NC = 1$. So, no visible differences are detected between the original and the recovered watermark.

In order to improve the correction of the recovered watermark, we insist in this version that the embedded watermark is binary coded on 0 and 1. So, it allows just two different intensities scale. Consequently, the used factor d to compute the PSNR between original and recovered watermark is equal to 2 and gives the present results in Tables 1 and 2.

Tables 1 and 2 show the effectiveness of the proposed watermarking approach to resist the different STIRMARK attacks. We note that the resistivity of the proposed approach against geometric attacks is very high. This efficiency is related to the properties of the Discreet Radon Transform. Also, the effectiveness of the proposed method to resist common image processing attacks is related to an accurate selection of the coefficients which are selected from the image in Radon field. These coefficients presenting the highest energy in the Radon field contain

Table 1: Resistance of the proposed method against the common image processing attacks

ATTACKS	NC	PSNR	BER	
			bits	percent
$Conv_2$	1	inf	0	0
$Median_3$	0.9878	71.0075	33	0.51
$Median_5$	0.9793	68.7107	56	0.875
$Median_7$	0.9841	69.8579	43	0.67
$PSNR_0$	0.9149	62.5942	229	3.578
$PSNR_50$	1	inf	0	0
$Noise_20$	0.9863	70.5106	37	0.578
$Noise_40$	0.9826	69.4716	47	0.73
$JPEG_50$	0.9413	63.9654	167	2.6
$JPEG_70$	0.9974	77.7416	7	0.109
$JPEG_80$	1	inf	0	0

the significant information of the original image, which allow the withstanding against the common image processing attacks. These coefficients are located and set on the line of projection, so they allow a good recuperation of transformed information with inverse radon transform. This robustness is mathematically proved in the following Section. The following images illustrate zoomed views of the selected coefficients in the Radon field "Figure 22" and the coded watermark in these coefficients illustrated in the figure "Figure 23".

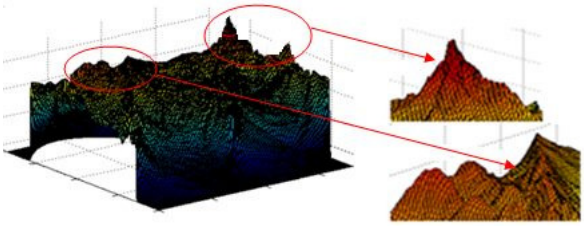

Figure 22: The used sets of coefficient to embed watermark in Radon field

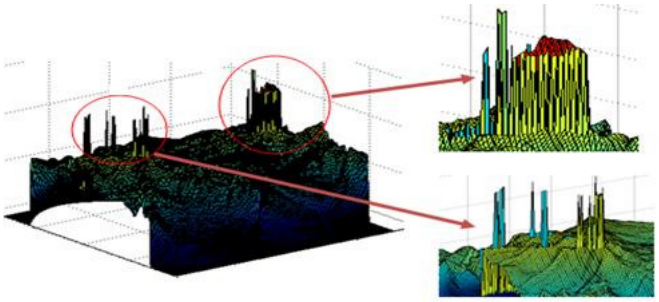

Figure 23: The sets of watermarked coefficient the watermark presence in the Radon field

In another hand, the watermarked image is illustrated in Figure 18. It represents an imperceptible watermarking scheme. We will prove in the following mathematical study why the watermarking system in radon field represents an imperceptible watermarking approach. In fact, embedding information in radon coefficient especially in the higher radon coefficients under the perceptibility threshold is defined by the Weber law. We note the data loss "error" between the recovered images after inverse radon transform of the original image $I'(x,y)$ and the watermarked image $I(x,y)$ by ε. The following equations prove that error has no visual effect on the watermarked image.

$$I^{'}(x,y) - I_w(x,y) = \varepsilon(x,y)$$

or the Weber law imposes that:

$$\sum_{i=1}^{M}\sum_{j=1}^{N}\frac{I^{'}(i,j) - I(i,j)}{I^{'}(i,j)} \leq \tau \qquad \text{where } \tau \cong (2\% - 3\%).$$

Since the simulation results proved that $\varepsilon < \tau$. So, perceptually we can say that no visible changes are engendered by the watermarking approach in radon domain, then:

$$I^{'} = I \qquad \text{and } \varepsilon \to 0.$$

Figures 24, 25, and 26 illustrate an original and Radon transformed image followed by the positions (In red) of the imperceptible distortions introduced by applying the radon transform and recovering the image by the inverse Radon transform without any watermark embedding.

Table 2: Resistance of the proposed method against the geometric attacks

ATTACKS	NC	PSNR	BER	
			bits	percent
$RESC_90$	0.9993	83.1828	2	0.03
$RESC_75$	0.9989	81.4214	3	0.046
$RNDDIST_1$	1	inf	0	0
$LARDIST$	1	inf	0	0
RML_10	1	inf	0	0
RML_40	0.9985	80.1720	4	0.06
$AFFINE_1$	1	inf	0	0
$AFFINE_8$	0.9996	86.1926	1	0.015
ROT_51	1	inf	0	0
$ROT_0.75$	0.9952	75.0532	13	0.2
ROT_1	1	inf	0	0
ROT_90	1	inf	0	0
$ROTCROP_0.5$	1	inf	0	0
$ROTCROP_1$	0.9996	86.1926	1	0.015
$ROTCROP_10$	1	inf	0	0
$ROTSCALE_0.5$	1	inf	0	0
$ROTSCALE_1$	1	inf	0	0
$SCALING_0.9$	0.9989	81.4214	3	0.046
$SCALING_0.7$	0.9896	71.7210	28	0.437

Figure 24: Original image

Figure 25: IDRT watermarked image

Figure 26: Difference between IDRT original image and IDRT watermarked image

In these Sections, we improve that the watermarking image in radon field presenting a more robustness against asynchronous attacks presented in table I is proved. In addition, when dealing with image, this transform doesn't engender any perceptual degradation.

4 Justifying Robustness Against Asynchronous Attacks

In this Section, we will detail why the proposed approach resists against the geometric attacks. This is done through the mathematical characteristics of the Radon transform.

The robustness of the proposed approach and its resistance against asynchronous attacks can be justified only if we prove mathematically that a change of the Radon matrix coefficients presented by a watermark insertion is invariant against geometric transforms and has no mathematical or visual impact on the image in its spatial representation. In addition, this transform has to be entirely reversible and conservative. In the case it is almost conservative, we have a loss of data in the inverse process when applying the inverse DRT. The data loss does not affect in any way the perceptibility of the watermarked image in the spatial domain based on the Weber law. All these constraints must be tested and proved in the following Section. Given an image $I(x,y)$ defined in $\Re_2^+$, $R(\rho,\theta)$ represents its radon projection in $\Re_2^+$. (x,y) and (ρ,θ) represent respectively the coordinates of the image in spatial and Radon domain.$[MN]$ and $[N_\rho N_\theta]$ represent the size of the image in spatial and Radon field. The invariance faces to the following geometric transforms have to be proved.

4.1 Linearity

Given $g(x,y) = \beta I(x,y)$ where β is a constant. The DRT of $g(x,y)$ gives the following relation:

$$DRT[g(x,y)] = R_1(\rho,\theta) \qquad \text{where } \frac{R_1(\rho,\theta)}{R(\rho,\theta)} = \beta^{'},$$

or $\beta^{'} = \beta + \Delta\beta$ through different tests we find that:

$$\begin{aligned} \Delta\beta << << << << \beta \qquad & \text{so } \beta^{'} \cong \beta. \\ Do:\ R_1(\rho,\theta) &= \beta R(\rho,\theta). \\ So:\ DRT[g(x,y)] &= \beta DRT[I(x,y)]. \end{aligned}$$

Similarly, we define the following relationship:

$$If:\ g(x,y) = \beta_1 I_1(x,y) + \beta_2 J(x,y).$$

The Radon Transformation of J gives the following results:

$$DRT[g(x,y)] = \beta_1 DRT[I_1(x,y)] + \beta_2 DRT[J(x,y)],$$

where $[I1(x,y)]$ and $[J(x,y)]$ are two image defined in spatial field and $\beta 1$ and $\beta 2$ are two constants. This relation proves that the DRT is linearly invariant.

4.2 Image Scaling

A scaling on the $\overrightarrow{X}$ and $\overrightarrow{Y}$ axis of the image is applied as presented in Figure 27 and the following equation:

$$g(x,y) = I(x - x_0, y - y_0).$$

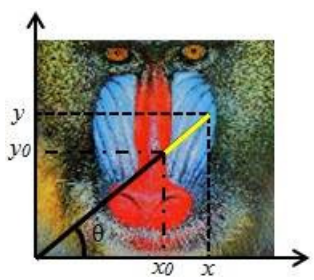

Figure 27: Scaling image on X and Y axis

The Radon transform of $J(x,y)$ is as follows:

$$DRT[g(x,y)] = R_1(\rho_1,\theta) = DRT[I(x - x_0, y - y_0)],$$

where

$$\begin{aligned}\rho_1 &= (x-x_0)\cos\theta + (y-y_0)\sin\theta \\ &= x\cos\theta - x_0\cos\theta + y\sin\theta - y_0\sin\theta \\ &= \underbrace{x\cos\theta + y\sin\theta}_{\rho} - x_0\cos\theta - y_0\sin\theta \\ &= \rho - x_0\cos\theta - y_0)\sin\theta.\end{aligned}$$

So:

$$DRT[g(x,y)] = R_1(\rho_1,\theta) = R(\rho - x_0\cos\theta - y_0\sin\theta, \theta).$$

Also, the error defined by $\Delta\rho = -x_0\cos\theta - y_0\sin\theta, \theta$ is lower than the value of ρ. Since the variation $\Delta\rho$ cannot allow the projection of a pixel neighbor defined by its coordinates (ρ,θ) due to its size $\Delta\rho <<<< \rho$ then, the radon transformation depends only on the value of ρ.

4.3 Image Rotation

Supposing that $K(\rho,\theta)$ represents the polar coordinate of $I(x,y)$ and $g(\rho,\theta) = K(\rho,\theta-\varphi)$ with φ represents the angle of circular shifting. The results of rotating a spatial image in the radon field is studied and presented in Figure 28 and the following equations:

$$\begin{aligned}DRT[g(\rho,\theta)] &= DRT[(\rho,\theta-\varphi)] = R_1(\rho_1,\theta_1) \\ &= I(x\cos\theta\cos\varphi + y\sin\theta\sin\varphi, \\ &\quad -y\cos\theta\sin\varphi + y\sin\theta\cos\varphi). \\ R_1(\rho_1,\theta_1) &= I(x\cos(\theta-\varphi), y\sin(\theta-\varphi)). \\ &= R(\rho,\theta-\varphi). \\ \rho_1 &= \rho \\ \theta_1 &= \theta-\varphi.\end{aligned}$$

So,

$$DRT[g(\rho,\theta)] = R_1(\rho_1,\theta_1) = R(\rho,\theta-\varphi).$$

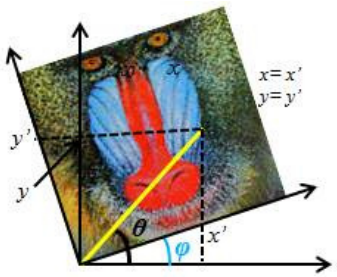

Figure 28: Circular shifted image by angle

This relation shows that the radon transform depends only on the value of $\theta-\varphi$ and its magnitude is constant. Consequently the projected pixel will change its location in the Radon field according to the angular rotation applied. This proves that angular rotations are conserved to generate the correspondent Radon coefficients.

4.4 Cropping Rotation and Scaling

In this section, we test the invariance of the DRT if different asynchronous attacks are combined simultaneously such as rotation and scaling or cropping without changing the axis projection.

Case 1. Scaling on Y axis and circular shifting by an angle (See Figure 29).

$$\begin{aligned}DRT[g(\rho,\theta)] &= DRT[K(\rho,\theta-\varphi)] = R_1(\rho_1,\theta_1) \\ &= I(x\cos\theta\cos\varphi + x\sin\theta\sin\varphi, \\ &\quad -(y-y_0)cos\theta\sin\varphi \\ &\quad +(y-y_0)\sin\theta\cos\varphi. \\ R_1(\rho_1,\theta_1) &= I(x\cos(\theta-\varphi), (y-y_0)\sin(\theta-\varphi)). \\ &= R(\rho - y_0\sin(\theta-\varphi), \theta-\varphi). \\ \rho_1 &= \rho - y_0\sin(\theta-\varphi) \\ \theta_1 &= \theta-\varphi.\end{aligned}$$

So, in this case:

$$DRT[K(\rho,\theta-\varphi)] = R(\rho - y_0\sin(\theta-\varphi), \theta-\varphi).$$

The error is defined by:

$$\Delta\rho = -y_0\sin(\theta-\varphi) <<<< \rho.$$

Experimental test proved that the error found is very small compared with ρ ($\Delta\rho <<<< \rho$).

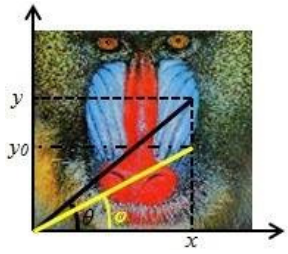

Figure 29: Scaling on Y axis and circular shifting by an angle

Case 2. Scaling on Xaxis and circular shifted of crop in image (See Figure 30).

$$\begin{aligned}DRT[g(\rho,\theta)] &= DRT[K(\rho,\theta-\varphi)] = R_1(\rho_1,\theta_1) \\ &= I((x-x_0)\cos\theta\cos\varphi \\ &\quad +(x-x_0)\sin\theta\sin\varphi, \\ &\quad -y\cos\theta\sin\varphi + y\sin\theta\cos\varphi. \\ R_1(\rho_1,\theta_1) &= I((x-x_0)\cos(\theta-\varphi), ysin(\theta-\varphi)) \\ &= R(\rho - x_0\cos(\theta-\varphi), \theta-\varphi) \\ \rho_1 &= \rho - x_0\cos(\theta-\varphi) \\ \theta_1 &= \theta-\varphi.\end{aligned}$$

So,

$$DRT[K(\rho,\theta-\varphi)] = R(\rho - x_0\cos(\theta-\varphi), \theta-\varphi).$$

The error is

$$\Delta\rho = -x_0\cos(\theta-\varphi) <<<< \rho.$$

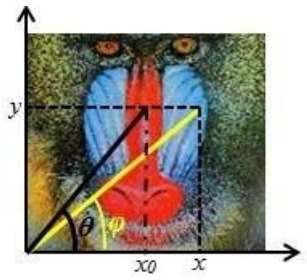

Figure 30: Scaling on Xaxis and circular shifted of crop in image

Case 3. Scaling on Xaxis and circular shifted of crop in image (See Figure 31).

$$\begin{aligned} DRT[g(\rho,\theta)] &= DRT[K(\rho,\theta-\varphi)] = R_1(\rho_1,\theta_1) \\ &= I((x-x_0)\cos\theta\cos\varphi \\ &\quad +(x-x_0)\sin\theta\sin\varphi, \\ &\quad -(Y-Y_0)\cos\theta\sin\varphi \\ &\quad +(Y-Y_0)\sin\theta\cos\varphi). \\ R_1(\rho_1,\theta_1) &= I((x-x_0)\cos(\theta-\varphi), \\ &\quad (Y-Y_0)\sin(\theta-\varphi)). \\ &= R(\rho-x_0\cos(\theta-\varphi) \\ &\quad -y_0\sin(\theta-\varphi),\theta-\varphi). \\ \rho_1 &= \rho-x_0\cos(\theta-\varphi)-y_0\sin(\theta-\varphi) \\ \theta_1 &= \theta-\varphi. \end{aligned}$$

So, in this case:

$$\begin{aligned} & DRT[K(\rho,\theta-\varphi)] \\ = \; & R(\rho-x_0\cos(\theta-\varphi),-y_0\sin(\theta-\varphi),\theta-\varphi). \end{aligned}$$

The error is defined by:

$$\Delta\rho = x_0\cos(\theta-\varphi)y_0\sin(\theta-\varphi).$$

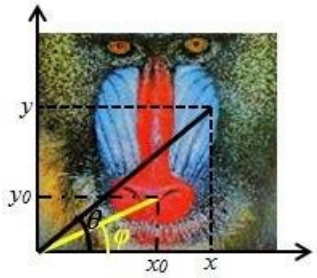

Figure 31: Scaling on X and T axis and circular shifted of crop in image

Due to its feeble value, the error $\Delta\rho$ cannot change the original integer quantized coefficient in Radon field. So, the used coefficient to code the watermark does not change and the watermark is correctly recovered. As proved above, face to singular or composed geometric transform, the Radon transform offers invariance to the transformed image. Consequently, the distortions and geometric transforms applied on the spatial watermarked image have generally no effect on the embedded watermark in the radon field since these variations are conserved over the Radon coefficients where the watermark is coded.

5 Comparative Study

In order to prove the efficiency and high robustness of the proposed method, a comparison study illustrated in Figures 32 and 33 is conducted with recent proposed approach in the literature exploiting the Radon domain [12] and [17].

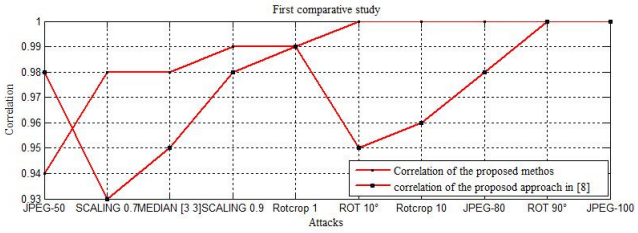

Figure 32: Comparative study between our proposed method and the developed technique in [12]

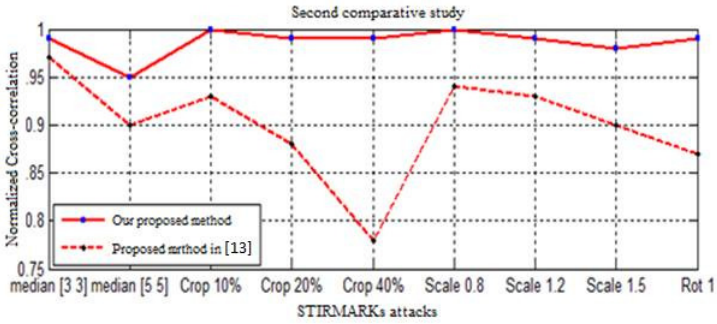

Figure 33: Comparative study between our proposed method and the Wang method in [17]

Compared to the proposed methods in [12] and [17], Figure 32 and Figure 33 show that the robustness of the proposed watermarking scheme in the radon field is more effective than the previous schemes. This efficiency is due to the propriety of radon field and its performance in detecting the important peaks by sing the inverse radon transform. The proposed watermarking scheme does not degrade the visual perception of the watermarked image and it is robust against the two categories of attacks.

6 Conclusions

In this paper a watermarking approach based on the Radon transform is presented. The watermark is coded in selected coefficients with respect to specific mathematical characteristics and the energy is characterized by

higher robustness against various attacks types. The proposed scheme presents high robustness especially against asynchronous attacks. This resistance against these geometric attacks is studied and proved mathematically. Accordingly, the equilibrium between watermarking constraints is achieved. Robustness and imperceptibility are respected and the embedding capacity is increased.

Acknowledgments

This study was supported by CEREP Research laboratory in College of Sciences and techniques in Tunisia. The authors gratefully acknowledge the anonymous reviewers for their valuable comments.

References

[1] A. Averbuch, I. Sedelnikov, and Y. Shkolnisky, "CT reconstruction from parallel and Fan-Beam projections by a 2-D discrete radon transform," *IEEE Transactions on Image Processing*, vol. 21, no. 2, pp. 733–741, 2012.

[2] L. Baisa and R. R. Manthalkar, "An overview of transform domain robust digital image watermarking algorithms," *Journal of Emerging Trends in Computing and Information Sciences*, vol. 2, no. 1, pp. 2079–8407, 2010.

[3] G. Beylkin, "Discrete radon transform," *IEEE Transactions on acoustics speech and signal processing*, vol. 35, no. 2, pp 162–172, 1987.

[4] C. C. Chang, K. F. Hwang, and M. S. Hwang, "A digital watermarking scheme using human visual effects," *Informatica: An International Journal of Computing and Informatics*, vol. 24, no. 4, pp. 505–511, 2000.

[5] C. C. Chang, K. F. Hwang, and M. S. Hwang, "A Feature-Oriented copyright owner proving technique for still images," *International Journal of Software Engineering and Knowledge Engineering*, vol. 12, no. 3, pp. 317–330, 2002.

[6] RSR. Channapragada, AS. Mantha, and Munaga V. N. K. Prasad, "Study of contemporary digital watermarking techniques," *IJCSI International Journal of Computer Science Issues*, vol. 9, no. 1, pp. 1694–0814, 2012.

[7] Y. Fu, "Robust oblivious image watermarking scheme based on coefficient relation," *International Journal for Light and Electron Optics*, vol. 124, no. 6, pp. 517–521, 2013.

[8] M. S. Hwang, C. C. Chang, and K. F. Hwang, "A watermarking technique based on One-way hash functions," *IEEE Transactions on Consumer Electronics*, vol. 45, no. 2, pp. 286–294, 1999.

[9] M. S. Hwang, C. C. Chang, and K. F. Hwang, "Digital watermarking of images using neural networks," *Journal of Electronic Imaging*, vol. 9, no. 4, pp. 548–555, 2000.

[10] G. Dayalin Leena, S. Selva Dhayanithy, and M. S. Hwang, "Robust image watermarking in frequency domain," *International Journal of Innovation and Applied Studies*, vol. 2, no. 4, pp. 582–587, 2013.

[11] L. Li, S. Li, A. Abraham, and J. S. Pan, "Geometrically invariant image watermarking using polar harmonic transforms," *Information Sciences*, vol. 199, pp. 1–19, 2012.

[12] I. Nasir, F. Khelifi, J. Jiang, and S. Ipson, "Robust image watermarking via geometrically invariant feature points and image normalisation," in *Proceeding of IET Image*, vol. 6, pp. 354, 2012.

[13] D. Simitopoulos, D. E. Koutsonanos, and M. G. Strintzis, "Robust image watermarking based on generalized radon transformations," *IEEE Transactions on Circuits and Systems for Video Technology*, vol. 13, no. 8, pp. 732–745, 2003.

[14] Q. Su, Y. Niu, X. Liu, and T. Yao, "A novel blind digital watermarking algorithm for embedding color image into color image," *International Journal for Light and Electron Optics*, vol. 124, no. 18, pp. 3254–3259, 2013.

[15] Q. Su, Y. Niu, X. Liu, and Y. Zhu, "A blind dual color image watermarking based on IWT and state coding," *Optics Communications*, vol. 285, no. 7, pp. 1717–1724, 2012.

[16] H. H. Tsaia, Y. J. Jhuanga, and Y. S. Lai, "An SVD-based image watermarking in wavelet domain using SVR and PSO," *Applied Soft Computing*, vol. 12, no. 8, pp. 2442–2453, 2012.

[17] E. Vahedi, R. A. Zoroofi, and M. Shiva, "Toward a new wavelet-based watermarking approach for color images using bio-inspired optimization principles," *Digital Signal Processing*, vol. 22, no. 1, pp. 153–162, 2012.

[18] W. W. Zhang, F. Gao, B. Liu, Q. Y. Wen, and H. Chen, "A watermark strategy for quantum images based on quantum fourier transform," *Quantum Information Processing*, vol. 12, no. 2, pp. 793–803, 2013.

Dhekra Essaidani was born in Bizerte, Tunis on 10 January 1989. In 2010, she received the Fundamental license in Electrical Engineering: Automatic and industrial computer from the ESTI (Tunis College of Technology and Computer science in Tunis) in Tunisia and Master degree in Electrical engineering (Automatic and industrial computer) from the ESSTT, in 2012.Since 2012; she enrolled in a doctoral thesis in the Department of Electrical Engineering in College of Sciences and techniques: CEREP Research laboratory. Here domain of interest is: Audio-image and video processing. Here main research interests are the multimedia security.

Hassene Seddik is born in 15 October 1970 in Tunisia, he has obtained the electromechanical engineer degree in 1995 and followed by the master degree in signal processing: speaker recognition and the thesis degree in image processing watermarking using non conventional

transformations. He has over 14 international journals papers and 65 conference papers. His domain of interest is: Audio-image and video processing applied in filtering, encryption and watermarking. He belongs to the CEREP research unit and supervises actually five thesis and 08 masters in the field.

Ezzedine Ben Braiek obtained his HDR on 2008 in Electrical engineering from ENSET Tunisia. He is, presently, full professor in the department of electrical engineering at the National High School of Engineering of Tunis (ENSIT) and manager of the research group on vision and image processing at the CEREP. His fields of interest include automatics, electronics, control, computer vision, image processing and its application in handwritten data recognition.